Acta Pharmaceutica Sinica B 2026;16(2):836−853

Chinese Pharmaceutical Association
Institute of Materia Medica, Chinese Academy of Medical Sciences

Acta Pharmaceutica Sinica B

www.elsevier.com/locate/apsb
www.sciencedirect.com

ORIGINAL ARTICLE

Gut microbiota drives the metabolic dysregulation in obesity-prone individuals by impairing GDCA-mediated activation of brown adipose thermogenesis and ileal GLP-1 secretion

Han Ma[a,b], Yuqi Wu[a,b], Delong Li[a,b], Haowen Sun[a,b], Yuan Xie[a,b], Shichun Zhao[a,b], Wenqian Guo[a,b], Meng Wang[a,b], Renyun Cui[b], Yanrong Huang[a,b], Xiankang Zhang[a,b], Jin-Yi Wan[a,b,*], Haiqiang Yao[a,b,*], Chun-Su Yuan[c,d]

[a]*School of Traditional Chinese Medicine, Beijing University of Chinese Medicine, Beijing 100029, China*
[b]*National Institute of TCM Constitution and Preventive Medicine, Beijing University of Chinese Medicine, Beijing 100029, China*
[c]*Tang Center for Herbal Medicine Research, The University of Chicago, Chicago, IL 60637, USA*
[d]*Department of Anesthesia and Critical Care, The University of Chicago, Chicago, IL 60637, USA*

Received 6 June 2025; received in revised form 21 September 2025; accepted 11 October 2025

KEY WORDS

Obesity-prone;
Gut microbiota;
Bile acids;
Glycodeoxycholic acid (GDCA);
TGR5;
Brown adipose;
Glucagon-like peptide-1 (GLP-1);
Glucolipid metabolism

Abstract Obesity-prone (OP) individuals exhibit an intrinsic predisposition to obesity and associated metabolic disorders, and early intervention in this population holds significant clinical value; however, the underlying mechanisms driving this susceptibility remain largely obscure. This study enrolled 46 OP subjects without diagnosed metabolic diseases and 35 healthy controls. Our findings revealed that, despite not reaching obesity diagnoses, OP subjects exhibited significant metabolic disturbances strongly associated with gut microbiota dysbiosis. They also displayed disturbed bile acid (BA) profiles, with depleted glycodeoxycholic acid (GDCA) identified as the most potent discriminator between the OP and healthy controls. Fecal microbiota transplantation (FMT) recapitulated metabolic dysfunction and BA pool remodeling, mediated by dysregulated hepatic expression of BA synthesis genes of *Cyp8a1*, *Cyp7a1*, and *Cyp7b1*. Notably, FMT-OP mice also phenocopied the diminished GDCA levels observed in OP subjects. GDCA supplementation in obese mice markedly improved body weight, hepatic steatosis, and metabolic dysfunction. Mechanistically, GDCA exerted anti-obesity effects by activating the TGR5

*Corresponding authors.
E-mail addresses: wanjinyi1128@163.com (Jin-Yi Wan), haiqiangyao@outlook.com (Haiqiang Yao).

Peer review under the responsibility of Chinese Pharmaceutical Association and Institute of Materia Medica, Chinese Academy of Medical Sciences.

https://doi.org/10.1016/j.apsb.2025.12.006

signaling, which enhanced brown adipose tissue (BAT) thermogenesis and stimulated ileal glucagon-like peptide-1 (GLP-1) secretion, thereby ameliorating obesity and associated metabolic dysregulation. Thus, these findings indicate that gut microbiota-driven dysregulation of BA signaling, particularly impaired TGR5 activation due to diminished GDCA, underlies glycolipid metabolic dysfunction in OP individuals.

1. Introduction

Obesity is a worldwide health concern and is a critical risk factor for type 2 diabetes, metabolic dysfunction-associated steatotic liver disease, hypertension, cardiovascular disease, and certain cancers[1-3]. Over the past four decades, the prevalence of obesity has nearly tripled worldwide and continues to escalate in many regions[1]. Despite similar diets, lifestyles, and environmental conditions, the susceptibility to obesity varies considerably. Some individuals, termed obesity-prone (OP), easily gain weight and suffer from obesity, while others do not. This phenomenon is also observed in rodents; under the same high-fat diet (HFD), some are sensitive to diet-induced obesity, indicating distinct susceptibilities to obesity[4,5]. Elucidating the molecular basis of OP may shed new light on the prevention and treatment of obesity-associated metabolic diseases.

The intestinal microbiota is increasingly recognized as a "metabolic organ" pivotal in regulating host metabolism[6-8]. Germ-free mice maintained under aseptic conditions exhibit resistance to diet-induced obesity[9,10]. Conversely, fecal microbiota transplantation (FMT) from obese donors can effectively reverse this condition, significantly increasing energy harvesting and reducing energy expenditure[11,12]. Furthermore, the gut microbiota can modulate the host metabolism through the production of microbial-derived metabolites. Bile acids (BAs) are end products derived from cholesterol, synthesized in the liver, and subsequently excreted into the intestine *via* the gallbladder. Primary BAs undergo biotransformation into secondary Bas through a series of processes facilitated by gut microbial enzymes, including deconjugation, dihydroxylation, and dehydrogenation of Bas within the distal small intestine and colon[13]. Altered BA compositions have been observed in obesity and various obesity-linked diseases[14-17]. For instance, the ratio of 12α-hydroxylated to non-12α-hydroxylated BAs has been reported to be elevated in Type 2 diabetes Mellitus (T2D) patients compared to non-T2D patients[18,19].

The G protein-coupled bile acid receptor 1 (GPBAR1 or TGR5) is a principal BA receptor that regulates metabolism[20]. TGR5 is expressed ubiquitously in immune cells and tissues across multiple metabolic organs; it is involved in various biophysiological processes and pathogenesis in metabolic disorders[21,22]. In brown adipose tissue (BAT), the triggering of BA-induced TGR5 signaling enhances energy expenditure through the type 2 iodothyronine deiodinase (D2)-mediated activation of thyroid hormone[23]. Notably, the activation of TGR5 in enteroendocrine L-cells prompts the secretion of glucagon-like peptide-1 (GLP-1), which subsequently stimulates insulin secretion to ameliorate glucose disorders and maintain energy homeostasis[24-26].

OP is a crucial internal driving force contributing to the development of obesity; however, its underlying mechanisms remain largely elusive. In the present study, we found that OP individuals exhibit metabolic derangements significantly associated with perturbations in gut microbiota and BA profiles, characterized by decreased glycodeoxycholic acid (GDCA) levels. FMT from OP subjects to antibiotics-treated mice effectively validated the pathogenic role of gut microbiota in the onset of obesity and disturbed BA pools, especially reduced GDCA concentration. Furthermore, GDCA treatment enhanced the thermogenesis of brown adipocytes and GLP-1 secretion in a TGR5-dependent manner. We aim to elucidate the characteristics and unveil the molecular mechanisms of OP subjects from the perspective of gut microbiota and BA profiles, potentially providing novel insights for the prevention and management of obesity preclinically.

2. Materials and methods

2.1. Human participants

Our research group has previously established a body constitution scale and the *National Standards of Classification and Determination of Constitution in Chinese Medicine* (ZYYXH/T157-2009), issued by the China Association of Chinese Medicine, to identify individuals of obesity-prone (OP), which is termed the phlegm-dampness (PD) body constitution in traditional Chinese medicine[27,28]. Detailed methodology for PD score calculation and the criteria used to identify OP subjects were provided in Supporting Information Table S1. Screened by the PD score, 46 OP subjects with no metabolic diseases were recruited in this study, and 35 healthy people were set as the healthy control (HC) group. Informed consent was obtained from all participants. This study was approved by the Beijing University of Chinese Medicine ethics committee (2022BZYLL0607) and performed following the Declaration of Helsinki. All participants were healthy individuals aged between 18 and 60 years with no diagnosed diseases, particularly metabolic disorders such as obesity, diabetes, metabolic syndrome, etc. Both groups maintained a regular diet and had not undergone antibiotic treatment in the preceding three months. Blood and fecal specimens were collected for subsequent assays.

2.2. Bacterial 16S rDNA gene sequencing

Fecal samples were procured immediately post-defecation and preserved at −80 °C. Bacterial DNA was extracted utilizing a DNeasy PowerSoil kit (Qiagen, Hilden, Germany) according to the manufacturer's protocols. The concentration and integrity of the DNA were confirmed using a NanoDrop 2000 spectrophotometer (Thermo Fisher Scientific, Waltham, MA, USA) and agarose gel electrophoresis, respectively. The extracted DNA was diluted to a concentration of 1 ng/μL and stored at −20 °C until further processing. PCR (Polymerase Chain Reaction) amplification of the V3−V4 hypervariable regions of the bacterial 16S rRNA gene was performed in a 25 μL reaction using universal

primer pairs (343 F: 5′-TACGGRAGGCAGCAG-3′; 798 R: 5′-AGGGTATCTAATCCT-3′). Amplicons were purified (Beckman Coulter Co., Brea, CA, USA) and quantified using the Qubit dsDNA assay kit (Thermo Fisher Scientific, Waltham, MA, USA), pooled at equimolar concentrations, and sequenced on an Illumina MiSeq platform (Illumina Inc., San Diego, CA, USA) by OE Biotech Company (Shanghai, China) following standard protocols. Paired-end reads were then preprocessed using Trimmomatic software, 19 to identify and trim ambiguous bases. After trimming, paired-end reads were assembled using FLASH software, 20. Clean reads were subjected to primer sequence removal and clustering to generate operational taxonomic units (OTUs) using Vsearch software with a 97% similarity cutoff.

2.3. Metabolomics analysis

After sample preparation and derivatization, BA profiles in fecal and plasma samples from OP and HC subjects were qualitatively and quantitatively analyzed using UPLC−ESI−MS/MS. The chromatographic separations were achieved on a Phenomenex Kinetex C18 column (2.1 mm × 100 mm, 2.6 μm; Phenomenex, Torrance, CA, USA). The detection parameters of the mass spectrometer were as follows. Curtain Gas: 35 psi; Collision-activated ionization (CAD) parameters: medium; Negative ion spray voltage: −4.5 kV; Ion source temperature, 450 °C, constant flow rate of 0.45 mL/min, and the column temperature was kept at 45 °C. Ion source: Gas1: 55 (psi); Gas2: 55 (psi). The metabolites were quantified by the Triple Quadrupole Mass Spectrometer's multiple reaction monitoring (MRM) detection mode.

2.4. Animal studies

All experimental protocols were approved by the Ethics Committee of the Beijing University of Chinese Medicine (BUCM-4-2021121001-4123). Male C57BL/6J mice aged six weeks were purchased from SPF (Beijing) Biotechnology Co., Ltd. (Beijing, China) and maintained under specific pathogen-free (SPF) conditions with free access to chow and water (temperature 20−22 °C, humidity 45 ± 5%, 12 h light/dark cycle). Food intake was monitored daily and used to calculate the energy intake of each mouse. The body weight was recorded weekly.

2.5. Antibiotic treatment and FMT

After one week of acclimatization, all mice received an antibiotic cocktail (ampicillin 1 mg/mL, neomycin 1 mg/mL, metronidazole

Table 1 Clinical characteristics of healthy controls and obesity-prone subjects.

Characteristics	Healthy control (n = 35)	Obesity-prone (n = 46)	P value
Age (years)	24.69 ± 2.11	24.67 ± 7.2	0.055$^{N.S.}$
Sex (male/female)	11/24	11/35	0.451$^{N.S.}$
Anthropometric parameters			
Weight (kg)	56.6 ± 9.84	72.1 ± 13.02	0.000***
Waist circumference (cm)	71.89 ± 7.91	86.13 ± 10.12	0.000***
Hip circumference (cm)	93.17 ± 6.76	102.28 ± 8.67	0.000***
BMI (kg/m^2)	20.44 ± 2.35	26.19 ± 4	0.000***
Waist: Height ratio	0.43 ± 0.04	0.52 ± 0.06	0.000***
Waist: hip ratio	0.77 ± 0.05	0.84 ± 0.07	0.000***
BFR (%)	21.8 ± 5.41	30.02 ± 5.3	0.000***
Glycemic control			
HbA1c (%)	5.2 ± 0.24	5.22 ± 0.25	0.721$^{N.S.}$
Fasting glucose (mmol/L)	4.12 ± 0.52	4 ± 0.45	0.306$^{N.S.}$
Fasting insulin (μIU/ml)	18.59 ± 5.05	27.59 ± 11.81	0.000***
GLP-1 (pmol/L)	10.88 ± 2.73	12.77 ± 2.61	0.012*
HOMA-IR	3.39 ± 0.98	4.94 ± 2.37	0.000***
QUICKI-IS	0.32 ± 0.01	0.31 ± 0.02	0.000***
TyG index	4.09 ± 0.28	4.24 ± 0.23	0.004**
Lipids			
Total cholesterol (mmol/L)	3.68 ± 0.73	3.54 ± 0.66	0.384$^{N.S.}$
HDL cholesterol (mmol/L)	1.32 ± 0.32	1.03 ± 0.23	0.000***
LDL cholesterol (mmol/L)	2.04 ± 0.59	2.19 ± 0.56	0.240$^{N.S.}$
Triglycerides (mmol/L)	0.63 ± 0.42	0.83 ± 0.39	0.002**
Triglyceride: HDL ratio	0.5 ± 0.33	0.87 ± 0.5	0.000***
LAP	7.36 ± 7.92	22.49 ± 13.64	0.000***
Non-HDL cholesterol (mmol/L)	2.35 ± 0.63	2.51 ± 0.63	0.286$^{N.S.}$
Others			
SBP (mmHg)	109.54 ± 10.78	113 ± 11.66	0.176$^{N.S.}$
DBP (mmHg)	73.29 ± 6.63	75.37 ± 7.79	0.208$^{N.S.}$
Heart rate (beats/min)	77.46 ± 8.18	80.35 ± 10.41	0.138$^{N.S.}$
BMR (calories/day)	1302.4 ± 215.2	1489 ± 235.34	0.000***

Data are represented as means ± SD or n (%) unless otherwise indicated. N.S., not significant; *$P < 0.05$, **$P < 0.01$, ***$P < 0.001$. Abbreviations: BMI, body mass index; BFR, body fat ratio; HbA1C, hemoglobin A1C; HOMA-IR, homeostatic model assessment for insulin resistance; QUICKI-IS, quantitative insulin sensitivity check index; TyG index, triglyceride glucose index; LDL cholesterol, low-density lipoprotein cholesterol; HDL cholesterol, high-density lipoprotein cholesterol; LAP, lipid accumulation product; SBP, systolic blood pressure; DBP, diastolic blood pressure; BMR, basal metabolic rate; SD, standard deviation.

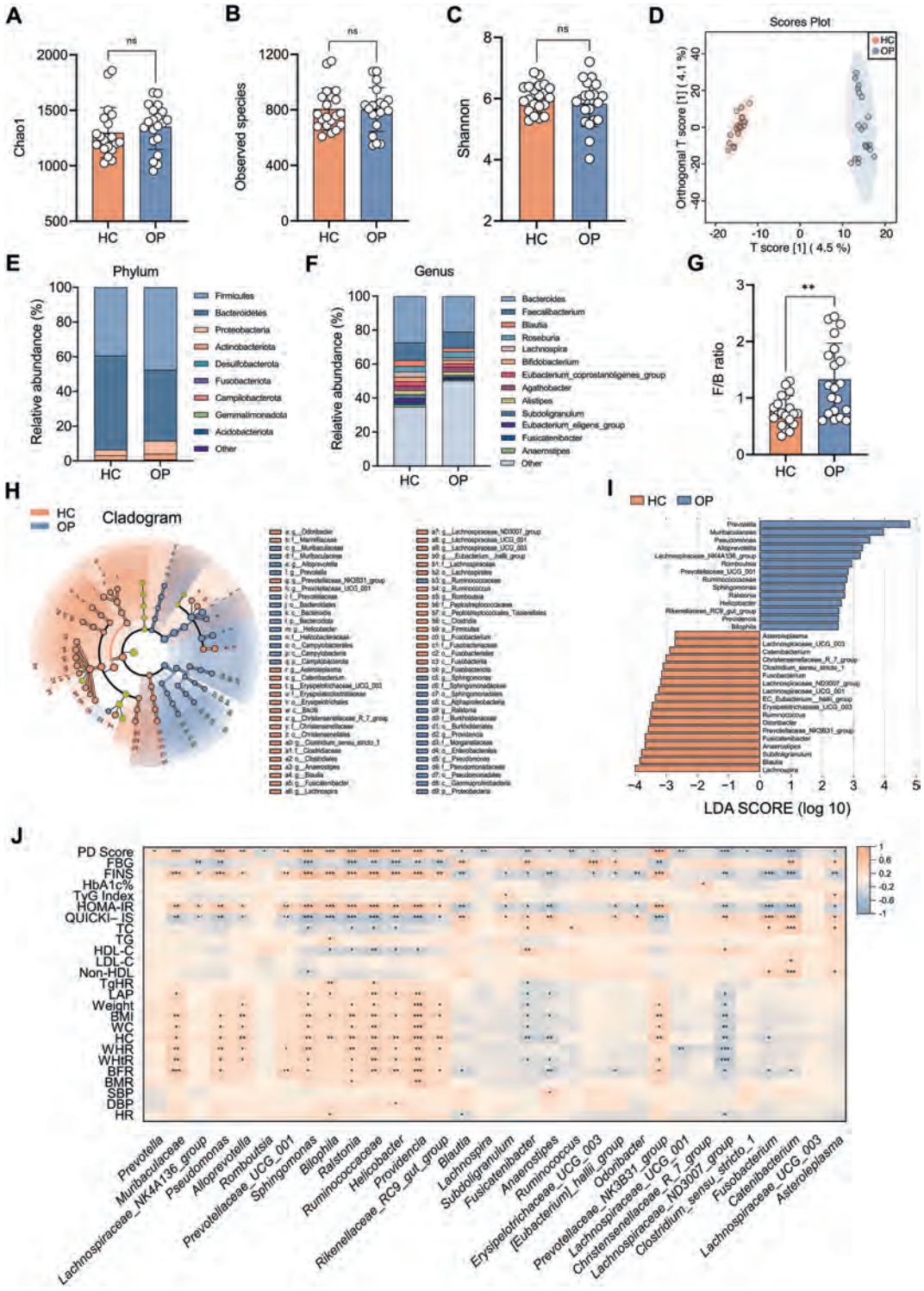

Figure 1 Obesity-prone individuals demonstrated distinct gut microbiota signatures compared with the healthy control group. Alpha diversity indices of the gut microbiota for HC and OP groups, including (A) Chao1 abundance, (B) Observed species, and (C) Shannon index. (D) OPLS-DA score plot of microbial abundance in fecal samples from HC and OP groups reveals a markedly distinct clustering pattern ($P < 0.01$, $n = 20$). Stacking plots of gut microbiota at the (E) Phylum and (F) Genus levels of HC and OP groups. (G) OP subjects demonstrated a significantly higher Firmicutes/Bacteroidetes ratio, suggesting dysbiosis of gut microbiota. (H) Cladogram generated by LEfSe displayed gut microbiota taxa of HC and OP groups. (I) LDA score for the bacterial taxa differentially abundant between HC and OP (LDA>2.5). (J) Correlation analysis revealed significant links between gut microbiota and clinical indicators. Abbreviations: HC, healthy control; OP, obesity-prone; OPLS-DA, orthogonal partial least squares discriminant analysis; LEfSe, Linear discriminant analysis Effect Size; LDA, linear discriminant analysis.

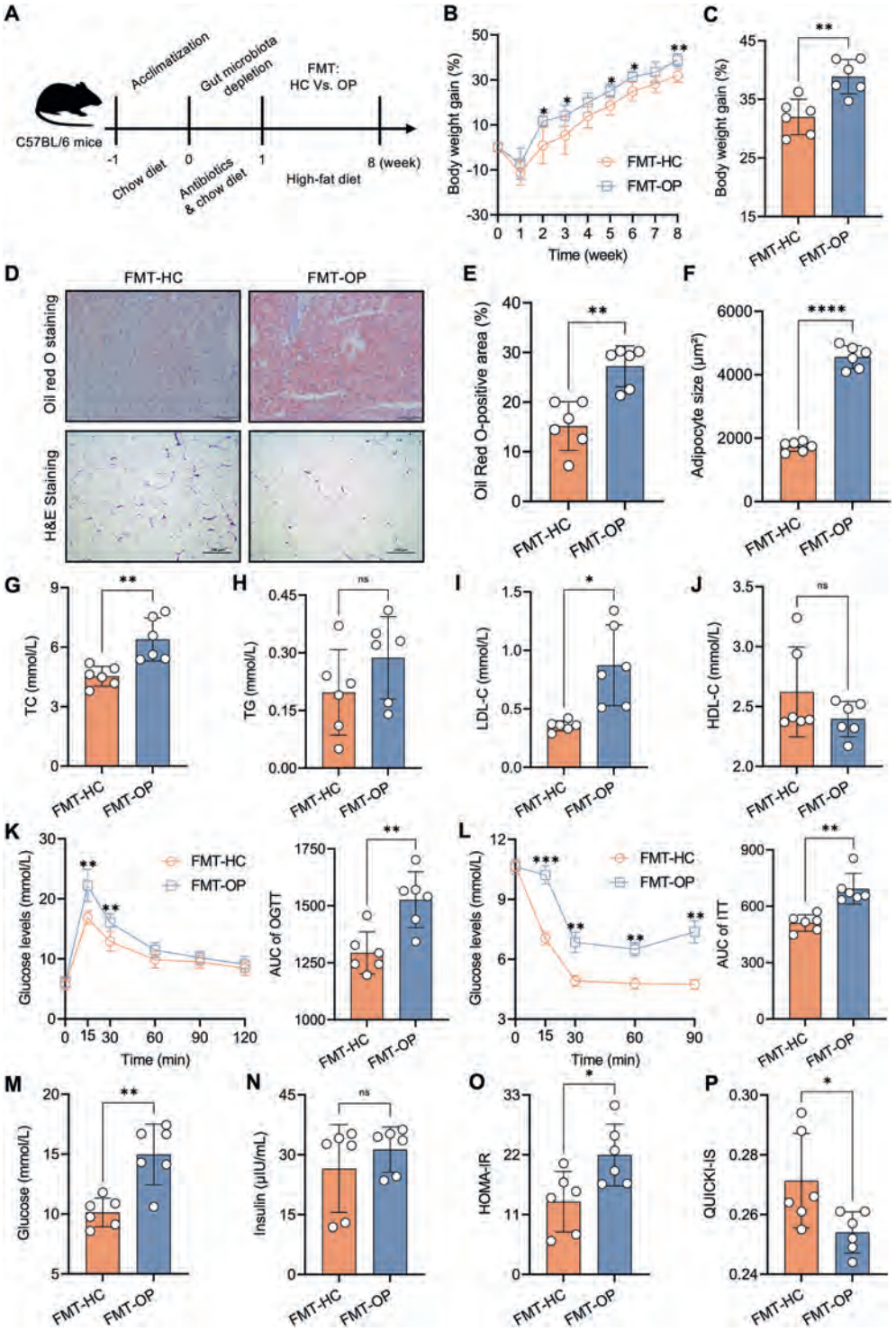

Figure 2 Fecal microbiota transplantation confirmed that the gut microbiota from obesity-prone individuals contributed to the predisposition to glycolipid dysmetabolism. (A) Experiment scheme. Body weight change curve (B) and the final body weight gain (C) of FMT-OP and FMT-HC groups. (D) Oil red O staining of liver tissue and H&E staining of epididymal fat (scale bars, 100 μm), accompanied by quantitative analysis of oil red O positive area (E) and size of adipocyte (F). Blood lipid indicators of TC (G), TG (H), LDL-C (I), and HDL-C (J) of FMT-OP and FMT-HC mice. Blood glucose level during the OGTT (K) and ITT (L) with corresponding calculated AUC. Glycemic parameters, including fasting blood glucose (M) and insulin (N), HOMA-IR (O), and QUICKI-IS index (P). The data are represented as means ± SD, $n = 6$. NS for $P > 0.05$, $^{*}P < 0.05$, $^{**}P < 0.01$, $^{***}P < 0.001$. Abbreviations: TC, total cholesterol; TG, triglyceride; LDL-C, low-density lipoprotein cholesterol; HDL-C, high-density lipoprotein cholesterol; OGTT, oral glucose tolerance test; ITT, insulin tolerance test; AUC, area under curve; HOMA-IR, homeostatic model assessment for insulin resistance; QUICKI-IS, quantitative insulin-sensitivity check index for insulin sensitivity.

0.25 mg/mL, and vancomycin 0.5 mg/mL) treatment in drinking water for seven days to deplete the gut microbiota[27]. For FMT, fecal samples from 12 subjects were randomly picked from each OP and HC group and then pooled within each group. 200 mg of feces were resuspended in 1.5 mL PBS and homogenized, then centrifuged at 800 rpm (Eppendorf 5424R centrifuge, Eppendorf, Hamburg, Germany) for 5 min, taking the supernatant as inoculum for transplantation. To minimize the transformations of microbial composition, the inoculum was prepared daily and then immediately administered by oral gavage to antibiotic-treated mice in a volume of 300 μL/day. During the FMT, all mice were fed a HFD (D12492, consisting of 60% fat, 20% carbohydrate, and 20% protein) purchased from SPF (Beijing) Biotechnology Co., Ltd. (Beijing, China).

2.6. GDCA administration

C57BL/6J mice were maintained under SPF conditions. An HFD-induced obesity model was employed. The treatment group received a daily oral gavage of GDCA dissolved in saline at 30 mg/kg/day[29], while the validation group was concurrently administered the same dose of GDCA and the TGR5 inhibitor SBI-115 (Bide Pharmatech Ltd., Shanghai, China) at a dose of 10 mg/kg/day[30]. In contrast, the control group was administered an equivalent volume of saline and fed a standard chow diet for four weeks. Prior to sacrifice, all mice were subjected to a fasting period and underwent both an oral glucose tolerance test (OGTT) and an insulin tolerance test (ITT). The OGTT was conducted by administering 1.0 g/kg of glucose orally, while the ITT was performed through the intraperitoneal injection of 0.75 U/kg insulin, and then blood glucose was tested subsequently at specific time points.

2.7. Cell experiments

C3H10T1/2 mesenchymal stem cells were maintained in MEM medium supplemented with 10% fetal bovine serum and 1% penicillin−streptomycin until reaching optimal confluence. For differentiation into brown adipocytes, C3H10T1/2 cells were treated for 2 days with induction medium containing 0.005 mmol/L dexamethasone (Bio-Rad Laboratories, Hercules, CA, USA), 0.05 μmol/L 3,3′,5-triiodo-L-thyronine (Yuanye Bio-Technology Co., Ltd., Shanghai, China; T3), 0.5 mmol/L 3-isobutyl-1-methylxanthine (Sigma−Aldrich, Darmstadt, Germany), 0.125 mmol/L indomethacin (Yuanye Bio-Technology Co., Ltd., Shanghai, China), 1 μmol/L rosiglitazone (Yuanye Bio-Technology Co., Ltd., Shanghai, China), and 0.005 μg/μL insulin (Solarbio Science & Technology Co., Ltd., Beijing, China). Subsequently, cells were transferred to maintenance medium containing 0.05 μmol/L T3, 1 μmol/L rosiglitazone, and 0.005 μg/μL insulin for 4 days, with medium changed every 48 h, resulting in fully differentiated brown adipocytes by Day 6.

STC-1 enteroendocrine cells were cultured in high-glucose DMEM supplemented with 10% fetal bovine serum and 1% penicillin−streptomycin. To investigate the cellular effects of GDCA, differentiated brown adipocytes and STC-1 cells were assigned to various treatment groups. Control groups were treated with DMSO alone. Brown adipocytes were exposed to GDCA at concentrations of 100 or 200 μmol/L, while STC-1 cells were treated with 80 or 160 μmol/L GDCA. Additional inhibitor groups received the same GDCA treatments along with 20 μmol/L SBI-115 for brown adipocytes or 80 μmol/L SBI-115 for STC-1 cells. Following a 24 h treatment period, both cell types were harvested and processed into appropriate sample formats for subsequent analysis.

2.8. Luciferase assays

C3H10T1/2 derived brown adipocytes and STC-1 enteroendocrine cells were seeded in 12-well plates, allowed to adhere overnight, before transfection using Lipofectamine 2000 reagent (Invitrogen, Waltham, MA, USA). Specifically, a mixture of 500 ng TGR5 luciferase reporter plasmid and 10 ng pGL-TK plasmid (Xianghong Biotechnology Co., Ltd., Beijing, China) was prepared in Opti-MEM medium, incubated for 20 min at room temperature, added to cells for 6 h, and then replaced with fresh complete medium. After an additional 24 h incubation, cells were administered: control groups received DMSO vehicle, while test groups were exposed to either 80 μmol/L GDCA (for STC-1 cells) or 100 μmol/L GDCA (for C3H10T1/2 cells), with a selective TGR5 agonist INT-777 serving as the positive control for 24 h to assess TGR5 activation[31]. Finally, cells were lysed with 150 μL passive lysis buffer per well, and luciferase activity was quantified using a dual-luciferase reporter assay kit (Beyotime Biotechnology Co., Ltd., Shanghai, China) on a SpectraMax Mini microplate reader (Molecular Devices, San Jose, CA, USA), where firefly luciferase signals (representing TGR5 activity) were normalized to Renilla luciferase (from pGL-TK) to account for transfection efficiency.

2.9. Histopathology staining

Paraffin-embedded sections of epididymal fat were stained with hematoxylin and eosin (H&E). Fat sections were deparaffined and dehydrated with xylenes and ethanol. Slides were thoroughly washed and dipped in hematoxylin, washed again with water and ethanol 95%, and incubated with eosin for 30 min. After incubation, sections were re-incubated with ethanol and xylenes and covered with a mounting medium. Parts of the left and medial lobes of the mouse liver were sampled for Oil Red O staining. Prepared with 4% paraformaldehyde fixative solution, liver sections (4 μm thick) were cut with a cryostat and rinsed with 60% isopropanol, stained with Oil Red O staining solution for 10 min, then rinsed with 60% isopropanol. Finally, sections were counterstained with hematoxylin. Images were analyzed using an inverted microscope system (Olympus, Tokyo, Japan).

2.10. RT-qPCR assays

Total RNA was extracted from different tissues using an RNA extraction reagent (Servicebio, Wuhan, China). cDNA was synthesized from 10 μg of total RNA utilizing Servicebio RT Enzyme Mix (Servicebio, Wuhan, China). Real-time PCR was conducted with 2 μL of the cDNA template added to 7.5 μL of 2 × SYBR Green qPCR Master Mix (None ROX) (Servicebio, Wuhan, China) and specific primers (2.5 μmol/L each). The expression of the target genes was quantified relative to that of an internal control gene (ACTIN) based on the comparison of the threshold cycle (CT) at constant fluorescence intensity. Relative expression (R) was calculated using Eq. (1):

$$R = 2^{-\Delta\Delta Ct} \quad (1)$$

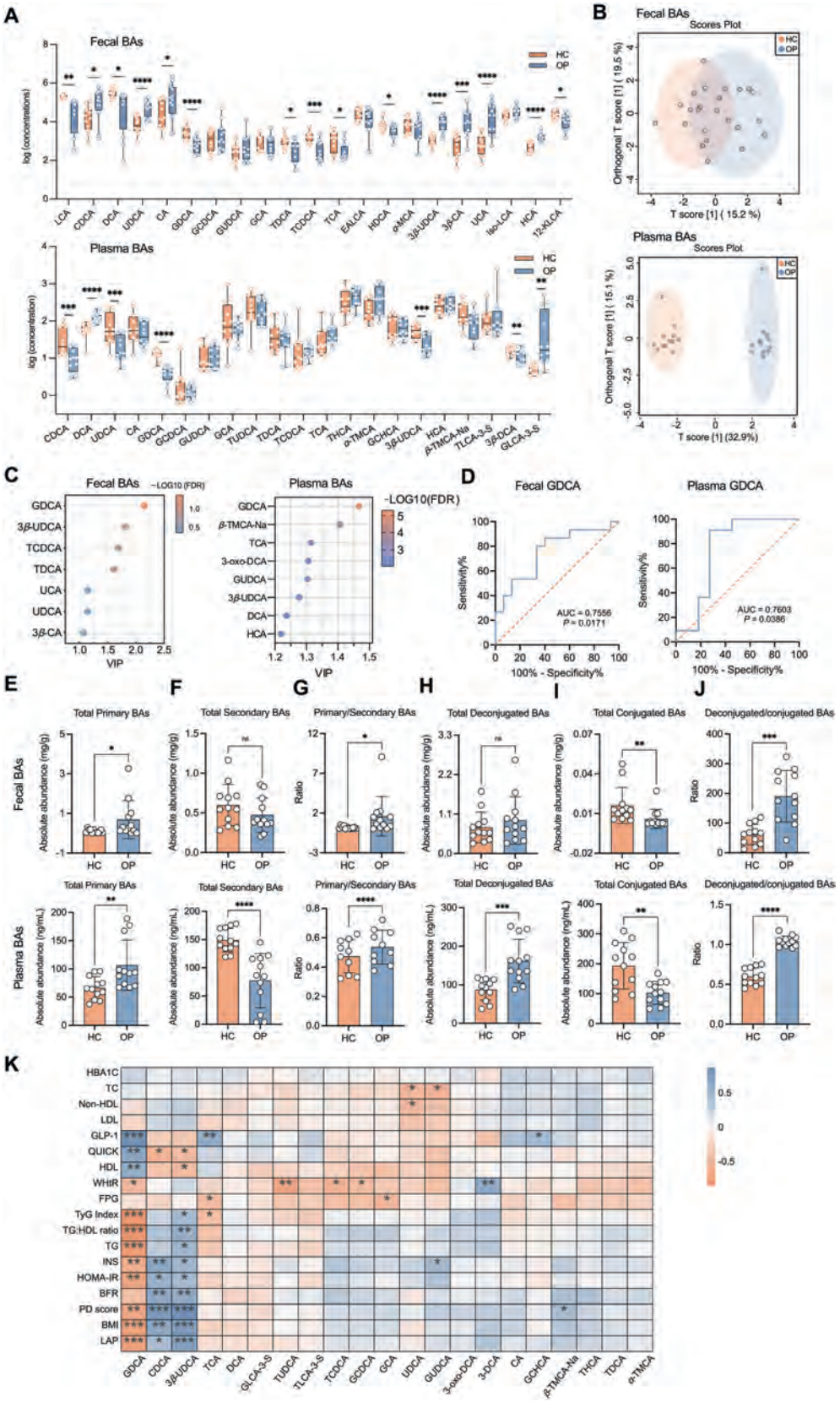

Figure 3 Obesity-prone subjects demonstrated altered bile acid profiles in both fecal and plasma samples. (A) Multiple BAs displayed significant changes between the OP and HC groups, including GDCA, CDCA, UDCA, etc. (B) OPLS-DA score plots indicated a clear separation between the OP and HC individuals, and (C) the VIP score identified GDCA as the most potent BA in discriminating OP subjects (Threshold: VIP>1), in both in fecal and plasma BAs. (D) The ROC curve confirmed the distinguished performance of GDCA in predicting OP individuals,

2.11. Statistical analysis

All data are represented as mean ± standard deviation (SD). The differences between two groups were compared using Student's *t*-test (unpaired, two-tailed). The differences among multiple groups were compared by using one-way analysis of variance (ANOVA) with Dunnett's *post hoc* test, while those tests were conducted only if F achieved $P < 0.05$ and there was no significant variance heterogeneity. The correlation was evaluated using Spearman's rank correlation coefficient. Data were analyzed using GraphPad Prism 9 software (GraphPad, San Diego, CA, USA). The statistical significance threshold was set at $P < 0.05$ and indicated as $^{*}P < 0.05$, $^{**}P < 0.01$, $^{***}P < 0.001$, respectively.

3. Results

3.1. Clinical characteristics of the obesity-prone and healthy control subjects

The characteristics of clinical participants are presented in Table 1. Despite all the OP subjects being free of metabolic diseases and most of the clinical indicators falling within normal ranges according to established diagnostic criteria, the body weight, BMI, waist-to-hip ratio, and multiple glucolipid indicators, including fasting insulin, HOMA-IR, TyG index, QUICKI-IS, and triglycerides, etc. were significantly higher in the OP group ($P < 0.01$), implying the predisposition to metabolic derangements. Notably, OP subjects exhibited significantly elevated GLP-1 concentrations, which aligned with previous reports, suggesting a physiological compensatory response in the early stage of obesity or metabolic syndrome[32,33]. Furthermore, correlation analysis revealed that the PD score was significantly correlated with multiple clinical indicators. Specifically, a positive correlation was found between the PD score and body weight, BMI, waist circumference, waist-to-hip ratio, body fat percentage, fasting insulin, HOMA-IR, TyG index, and triglycerides, etc., while a negative correlation was observed with QUICKI-IS and HDL cholesterol levels (Supporting Information Fig. S1), which also demonstrated the reliability of the PD score in identifying OP individuals.

3.2. The distinct gut microbiota compositions of obesity-prone individuals were significantly correlated with multiple metabolic parameters

Over the past few decades, mounting evidence has revealed the crucial role of gut microbiota perturbations in the development of obesity and metabolic diseases[34]. To uncover the underlying pathological basis of the differential metabolic phenotype of the HC and OP subjects, we performed 16S rDNA sequencing to detect the gut microbiota composition of the two groups. No significant difference in bacterial alpha diversity between the HC and OP groups was observed (Fig. 1A−C). Notably, the orthogonal partial least squares discriminant analysis (OPLS-DA) demonstrated a distinct clustering pattern between subjects from the OP and HC groups (Fig. 1D). The degree of taxonomic abundance at the phylum and genus level was examined to evaluate the overall composition of the bacterial community. Compared to the HC, the OP group showed significantly different relative abundance at both the phylum and genus levels (Fig. 1E and F).

Moreover, the significantly elevated Firmicutes/Bacteroidetes ratio suggested a gut microbiota dysbiosis in OP individuals (Fig. 1G). The linear discriminant analysis (LDA) effect size (LEfSe) was further used to identify differentially abundant taxa between the two groups. Notably, *Prevotella* was found to be the signature gut microbiota genus in the OP group, which was reported to be closely correlated with metabolic diseases[35] (Fig. 1H and I). Correlation analysis, as shown in the heatmap, identified the significant association between differently abundant gut microbiota genera and various metabolic clinical indicators (Fig. 1J), which implies that gut microbiota might be germane to the physiopathology of OP.

3.3. Fecal microbiota transplantation validated the pivotal role of gut microbiota in the dysmetabolism susceptibility of obese-prone subjects

To further explore the role of gut microbiota in predisposing OP subjects to metabolic disturbances, we conducted a FMT experiment. An antibiotic cocktail treatment was applied to C57BL/6J mice to deplete most of the gut microbiota[27]. Microbial inoculum from OP and HC fecal samples was administered orally to antibiotic-treated recipient mice under a HFD (Fig. 2A). The FMT-OP mice exhibited elevated body weights by the end of the first week, and this trend was consistently maintained (Fig. 2B), resulting in a significantly higher body weight gain than the FMT-HC group (Fig. 2C). Pathological staining also identified significantly enhanced liver fat accumulation and hypertrophic white adipocytes in FMT-OP mice (Fig. 2D−F). Serum total cholesterol (TC) and low-density lipoprotein cholesterol (LDL-C) increased significantly in the FMT-OP group (Fig. 2G−J), suggesting that OP gut microbiota induced abnormality in lipid metabolism.

Furthermore, FMT-OP mice also exhibited remarkable dysglycemia. Glucose and insulin tolerance were markedly impaired in the FMT-OP mice, as shown by the OGTT and ITT, respectively (Fig. 2K and L). Although fasting serum insulin was similar in the FMT-OP and FMT-HC groups, the FMT-OP mice had significantly elevated fasting blood glucose and HOMA-IR index, with declined QUICKI-IS index levels (Fig. 2M−P). In a nutshell,

AUC = 0.76. OP individuals displayed distinct fecal and plasma BA characteristics in (E) total primary BAs, (F) total secondary BAs, (G) the ratio of total primary bile acids to total secondary BAs, (H) total deconjugated BAs, (I) total conjugated BAs and (J) the ratio of total deconjugated bile acids to total conjugated BAs. (K) Correlation analysis revealed significant links between plasma BAs and clinical indicators. The data are represented as means ± SD, $n = 12$; NS for $P > 0.05$, $^{*}P < 0.05$, $^{**}P < 0.01$, $^{***}P < 0.001$, $^{****}P < 0.0001$. Abbreviations: BA, bile acid; GDCA, glycodeoxycholic acid; LCA, lithocholic acid; CDCA, chenodeoxycholic acid; DCA, deoxycholic acid; VIP, variable importance in projection; ROC, receiver operating characteristic; BW, body weight; TC, total cholesterol; TG, triglyceride; HDL, high density lipoprotein; LDL, low density lipoprotein; FPG, fasting plasma glucose; TyG Index, triglyceride glucose index; Ins, insulin; HOMA-IR, homeostatic model assessment for insulin resistance; QUICKI, quantitative insulin sensitivity check index; BFR, body fat ratio; BAT, brown adipose tissue; iWAT, inguinal white adipose tissue; PAT, perirenal white adipose tissue; eWAT, epididymal white adipose tissue; GLP-1, glucagon-like peptide-1; LAP, lipid accumulation product.

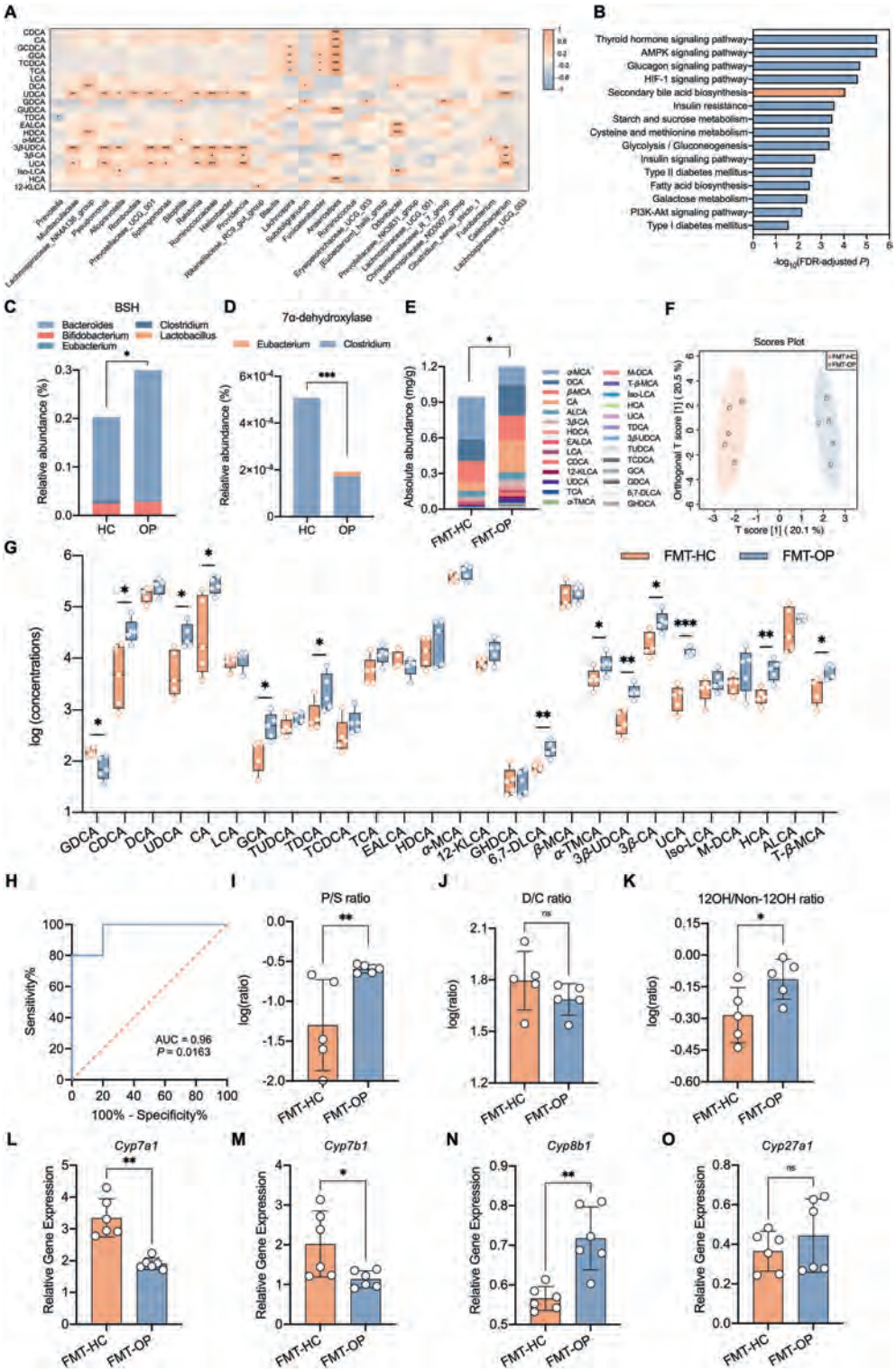

Figure 4 Gut microbiota from obesity-prone individuals contributed to the bile acid dysregulation in FMT-OP and FMT-HC mice. (A) Correlation analysis revealed significant links between fecal bile acids and gut microbiota. (B) Predicted KEGG functional pathway differences at level 3 inferred from 16S rDNA gene sequences using PICRUSt2 between the OP and HC groups. Relative abundance of bacterial genera expressing specific enzymes involved in the production of secondary BAs: (C) the gut bacteria that express bile salt hydrolase (BSH), (D) the gut bacteria known to express 7-α-dehydroxylase. (E) The absolute abundance of fecal bile acids (mg/g) in FMT-HC and FMT-OP groups. (F) OPLS-DA score plot of species abundance in fecal samples from FMT-HC and FMT-OP groups reveals a markedly distinct clustering pattern. (G) Multiple BAs displayed significant changes between the FMT-HC and FMT-OP groups, including GDCA, CDCA, UDCA, CA, etc. ($n = 5$). (H) The ROC curve confirmed the distinguished performance of GDCA in predicting FMT-OP individuals, AUC = 0.96. The three main ratios of fecal bile acids were considered: (I) the ratio of total primary bile acids to total secondary bile acids, (J) the ratio of total deconjugated bile acids to

these data suggested that the gut microbiota from OP individuals might lead to dysregulated glycolipid metabolism and insulin resistance.

3.4. Obesity-prone subjects exhibited disturbed bile acid profiles, with GDCA identified as the most potent discriminator between the two groups

As a key class of microbiota-derived metabolites, BAs play a critical role in the development of obesity and metabolic diseases. A UPLC−ESI−MS/MS approach was applied to quantitate both the fecal and plasma BA profiles of OP and HC groups. Multiple BAs exhibited significantly different concentrations. Specifically, in the fecal BAs, lithocholic acid (LCA), deoxycholic acid (DCA), GDCA, taurodeoxycholic acid (TDCA), taurochenodeoxycholic acid (TCDCA), taurocholic acid (TCA), hyodeoxycholic acid (HDCA), and 12-ketolithocholic acid (12-KLCA) were significantly decreased in the OP group, and most of the differential BAs belonged to the secondary and conjugated BA categories. Conversely, the primary BAs, including chenodeoxycholic acid (CDCA), ursodeoxycholic acid (UDCA), cholic acid (CA), 3β-cholic acid (3β-CA), ursocholic acid (UCA), and hyocholic acid (HCA) demonstrated increased concentrations in the OP group (Fig. 3A). In the plasma BAs, CDCA, UDCA, DCA, GDCA et al., also demonstrated significant difference between OP and HC subjects (Fig. 3A). Moreover, a distinct clustering was observed in the OPLS-DA score plot in both fecal and plasma BAs (Fig. 3B). OP subjects had markedly reduced GDCA concentrations in both fecal and plasma samples. Furthermore, GDCA was identified as the most potent BA in discriminating the OP and HC groups based on the variable importance in projection (VIP) scores (Fig. 3C). The receiver operating characteristic (ROC) curve displayed excellent discrimination of GDCA (AUC = 0.76, Fig. 3D), which further verified the results of the VIP score.

The BA pool of OP subjects had notably increased total primary BA concentrations in both fecal and plasma BAs (Fig. 3E and F), and the primary-to-secondary BA ratio also increased significantly in the OP group (Fig. 3G). The OP group exhibited elevated levels of total deconjugated BAs alongside a reduction in conjugated BAs, resulting in a corresponding increase in the deconjugated-to-conjugated BA ratio (Fig. 3H−J). Spearman correlation analyses were performed to elucidate the association between plasma BA levels and clinical parameters. As revealed in the heatmap, BAs exhibited significant correlations with multiple metabolic indicators, and GDCA had significantly negative correlations with body weight, BMI, and waist circumference, while it showed a notable positive correlation with GLP-1 levels (Fig. 3K).

3.5. Gut microbiota of obesity-prone individuals drove the bile acid dysregulation and decreased the GDCA concentration

The production of secondary BAs is regulated by the gut microbiota through the action of bile salt hydrolase (BSH) and 7α-dehydroxylase. As displayed in Spearman's correlation analysis, gut microbiota had a significant association with BAs (Fig. 4A). The gut microbiota can modulate the host metabolism *via* various signaling pathways. To further elucidate the functional prediction and pathway inferences of the differential intestinal flora of OP subjects, the Phylogenetic Investigation of Communities by Reconstruction of Unobserved States (PICRUSt2) approach was employed. The results indicated that multiple metabolic pathways were enriched, including the AMPK, glucagon, and insulin resistance signaling, etc. Notably, secondary bile acid biosynthesis pathway was also a critical differential signal pathway of gut microbiota between the OP and HC individuals (Fig. 4B). In the intestine, gut bacteria BSH deconjugates conjugated bile acids, then bacterial 7α- and 7β-dehydroxylases convert the primary BAs to secondary BAs[36]. We examined the bacterial taxa that conduct the key steps of secondary BA biosynthesis[37,38], and found that the gut bacteria that express BSH were increased in OP individuals (Fig. 4C), while the gut bacteria known to express 7α-dehydroxylases were significantly decreased (Fig. 4D).

To further verify the effects of gut microbiota on BA profile, FMT validation was conducted. Interestingly, the FMT-OP and -HC mice exhibited similar plasma BA compositions to the OP and HC subjects (Fig. 3B), with the FMT-OP group having significantly elevated absolute BA abundances (Fig. 4E). The OPLS-DA score plot also revealed a distinct clustering pattern between samples from the FMT-OP and FMT-HC groups (Fig. 4F). A variety of BAs displayed different levels between the two groups. Notably, GDCA was significantly lowered in the FMT-OP group (Fig. 4G), implying that the gut microbiota effectively phenocopied the dysregulated BA profiles of OP subjects. The ROC curve also confirmed the excellent predictive ability of GDCA for the distinction between FMT-OP and FMT-HC mice (AUC = 0.96, Fig. 4H). Furthermore, the BA composition analysis revealed that the FMT-OP group was characterized by a markedly elevated primary-to-secondary ratio (Fig. 4I), in line with that of the clinical OP subjects. The ratio of deconjugated to conjugated BAs did not change significantly between the two groups (Fig. 4J). However, the ratio of 12OH to non-12OH BAs demonstrated a notable increase in the FMT-OP group (Fig. 4K), suggesting the gut microbiota from OP subjects had largely shifted the BA biosynthesis towards the classical BA synthesis pathway in the liver. Therefore, we further examined the hepatic expression of genes related to BA synthesis (Fig. 4L−O). Of note, *Cyp7a1*, the rate-limiting enzyme in BA synthesis, demonstrated decreased gene expression in the livers of the FMT-OP group (Fig. 4L). Furthermore, down-regulated expression of *Cyp7b1* (Fig. 4M) and up-regulated expression of *Cyp8a1* were observed in the FMT-OP group (Fig. 4N), which confirmed that the classical pathway is the predominant BA synthesis route of FMT-OP mice.

3.6. GDCA ameliorated obesity linked metabolic dysfunction and remodeled the bile acid pool in a TGR5-dependent manner

Both OP subjects and FMT-OP mice exhibited the characteristic of deficient GDCA, and consequently, we proceeded to investigate the potential metabolic modulation effects of GDCA in a high-fat diet-induced obesity (DIO) mouse model. Given that the receptor TGR5 has been reported to play a pivotal role in mediating BAs'

total conjugated bile acids, and (K) the ratio of 12α-hydroxylated primary BA to the non-12α-hydroxylated primary BA for FMT-HC and FMT-OP groups. The hepatic expression of genes related to BA synthesis, including (L) *Cyp7a1*, (M) *Cyp7b1*, (N) *Cyp8b1*, and (O) *Cyp27a1* in FMT-HC and FMT-OP mice. The data are represented as means ± SD, $n = 6$, and NS for $P > 0.05$, $^{*}P < 0.05$, $^{**}P < 0.01$, $^{***}P < 0.001$.

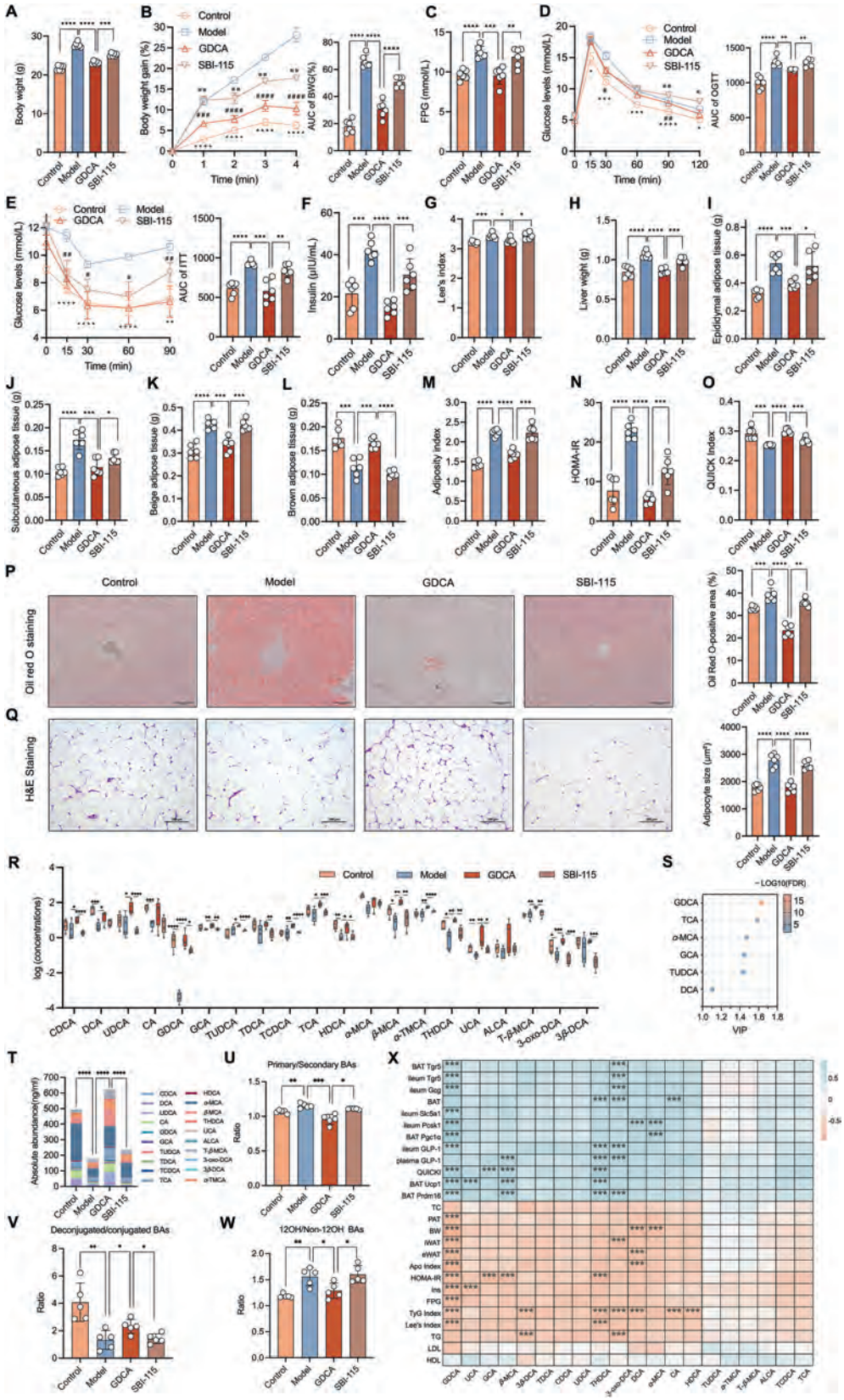

Figure 5 GDCA treatment reversed the obesity-related symptoms in high-fat diet-induced obesity mouse model and remodeled the plasma bile acid profiles. Mice in the treatment group were gavaged with GDCA (30 mg/kg/day), and the validation group mice were co-administrated with GDCA (30 mg/kg/day) plus a TGR5 inhibitor SBI-115 (10 mg/kg/day). (A) Body weight at the end of this 4-week study. (B) Changes in body weight gain with corresponding calculated AUC. (C) Fasting plasma glucose levels. Blood glucose level during the OGTT (D) and ITT (E) with

metabolic regulation[31,39], we set a validation group by co-administering GDCA with a selective TGR5 antagonist SBI-115[30]. Administration of GDCA significantly counteracted diet-induced obesity and related metabolic disturbances. Following a four-week intervention, GDCA-treated mice exhibited a marked reduction in body weight compared to obese controls (Fig. 5A and B). GDCA treatment substantially improved systemic glucose homeostasis. Fasting blood glucose levels were significantly lowered (Fig. 5C). Furthermore, GDCA-enhanced insulin sensitivity and glucose tolerance were evidenced by improved performances during both OGTT (Fig. 5D) andITT (Fig. 5E). Consistent with these metabolic improvements, circulating insulin levels were reduced (Fig. 5F), leading to a significant decrease in HOMA-IR index (Fig. 5N) and an increase in the QUICKI index (Fig. 5O).

The anti-obesity effects of GDCA were further reflected in altered body composition. Lee's index, a measure of obesity, was significantly lower in the treatment group (Fig. 5G). This was accompanied by a decreased adiposity index (Fig. 5M) and smaller mass of major fat depots, including epididymal white adipose, subcutaneous white adipose, and beige adipose tissue (Fig. 5I−K). Liver weight was also reduced (Fig. 5H), whereas brown adipose tissue mass increased substantially (Fig. 5L). Histological analyses provided direct morphological evidence of GDCA's efficacy. Oil Red O staining of liver sections revealed a dramatic reduction in lipid droplet accumulation, indicating alleviation of hepatic steatosis (Fig. 5P). Concordantly, histological examination of epididymal white adipose tissue *via* H&E staining showed a noticeable decrease in adipocyte size, signifying a reduction in fat storage (Fig. 5Q).

GDCA administration also induced a profound remodeling of circulating BA pools (Fig. 5R). Plasma GDCA levels were markedly elevated following the treatment, with GDCA identified as the potent discriminator to separate from the obesity model group (Fig. 5S). A stacked plot confirmed the shift in the compositional landscape of plasma BA profiles (Fig. 5T), accompanied by decreased primary-to-secondary BA (Fig. 5U) and 12OH/non-12OH BA ratios (Fig. 5W), along with an increased deconjugated-to-conjugated BA ratio (Fig. 5V). Correlation analysis demonstrated that the circulating GDCA concentrations were significantly associated with critical indicators of enhanced metabolic health, including reduced body weight, lowered fasting glucose, and improved insulin sensitivity (Fig. 5X). Moreover, GDCA levels correlated positively with *Tgr5* gene expression in both BAT and ileum. They were also associated with genes involved in BAT thermogenesis and ileal GLP-1 secretion, as illustrated in Fig. 5X. These findings suggest a pivotal role for TGR5 in mediating the therapeutic effects of GDCA.

Notably, the metabolic benefits conferred by GDCA were abolished upon co-administration with the TGR5 inhibitor SBI-115, confirming that the observed effects are mediated specifically through the TGR5 signaling.

3.7. GDCA activated the TGR5 signaling, thereby enhancing brown adipose tissue thermogenesis and ileal GLP-1 secretion in mice with diet-induced obesity

Administration of GDCA significantly activated TGR5 signaling in BAT of diet-induced obesity mice, as demonstrated by elevated immunofluorescence staining and quantitative fluorescence intensity of TGR5 (Fig. 6A and B). Consistent with these observations, *Tgr5* gene expression and cAMP concentration were markedly increased (Fig. 6C and D), confirming receptor activation. Consequently, key thermogenic markers including *Ucp1*, *Pgc-1α*, and *Prdm16* were substantially upregulated (Fig. 6E−G), indicating enhanced thermogenic capacity of BAT. Further morphological analysis revealed that GDCA treatment promoted mitochondrial biogenesis and lipid utilization. Immunofluorescence staining of BAT sections revealed smaller lipid droplets and a more multilocular morphology, and pronounced reduction in lipid droplet (LD) number per cell (Fig. 6O and P). Accompanied by an increase in mitochondrial fluorescence intensity (Fig. 6Q), and a higher proportion of LD−mitochondria contacts, exhibiting a perilipin-encircled distribution and forming tight clusters (Fig. 6R). These structural changes enhance lipid mobilization, enable direct fatty acid transfer to mitochondria, and bypass cytosolic diffusion, thereby ensuring efficient substrate channeling for β-oxidation.

Parallel activation of TGR5 was observed in the ileum, with increased immunofluorescence signal and quantitative intensity of TGR5 (Fig. 6H and I), and accompanied by elevated *Tgr5* expression and cAMP levels (Fig. 6J and K), confirming functional receptor engagement. Accordingly, genes critical for GLP-1 biosynthesis and secretion, *e.g.*, *Gcg*, *pcsk1*, and *Slc5a1* were significantly upregulated (Fig. 6L−N). This molecular response translated into enhanced GLP-1 production, as visualized by immunofluorescence staining of ileal tissues (Fig. 6S and T) and quantified *via* ELISA in both plasma and ileum samples (Fig. 6U and V).

Collectively, these findings indicate that GDCA elicits its metabolic effects *via* tissue-specific activation of TGR5, by enhancing thermogenesis in BAT and stimulating GLP-1 secretion from the ileum. The abrogation of all phenotypic and biochemical outcomes by the selective antagonist SBI-115 underscores the essential role of TGR5 signaling in mediating these responses. Further *in vitro* validation of these findings will be detailed in the following section.

3.8. In vitro models confirmed that GDCA augmented thermogenesis in brown adipocytes and GLP-1 secretion from enteroendocrine cells in a TGR5-dependent manner

Cell experiments were performed to verify the critical role of TGR5 in mediating GDCA's therapeutic effects. First, we assessed the impact of GDCA on thermogenesis using brown adipocytes differentiated from C3H10T1/2 mesenchymal stem cells. The dual

corresponding calculated AUC. (F) insulin. (G) Lee's index. Weight of liver (H), epididymal white adipose (I), subcutaneous white adipose (J), beige adipose tissue (K), and brown adipose tissue (L). (M) Adiposity index. (N) HOMA-IR. (O) QUICK index. Representative photomicrographs and quantitative analyses of (P) Oil Red O-stained liver sections and (Q) H&E-stained epididymal adipose tissue (scale bars: 100 μm). (R, S) Plasma BA profiles were quantified by UPLC−MS/MS at the endpoint. (R) GDCA treatment significantly altered the concentrations of the BA pool. (S) VIP scores identified GDCA as the most potent discriminator. (T) Stacked plot of BA profiles. GDCA treatment modulated the features of (U) primary to secondary BA ratio, (V) deconjugated to conjugated BA ratio, and (W) 12OH to non-12OH BA ratio. (X) Plasma GDCA levels demonstrated significant correlations with multiple metabolic indicators. The data are represented as means ± SD, $n = 6$; NS for $P > 0.05$, $^{*}P < 0.05$, $^{**}P < 0.01$, $^{***}P < 0.001$, $^{****}P < 0.0001$. For panels B, D, and E, the symbols * indicate statistically significant differences for the Control *vs.* Model, $^{\#}$ for GDCA *vs.* Model, and $^{※}$for SBI-115 *vs.* GDCA comparisons.

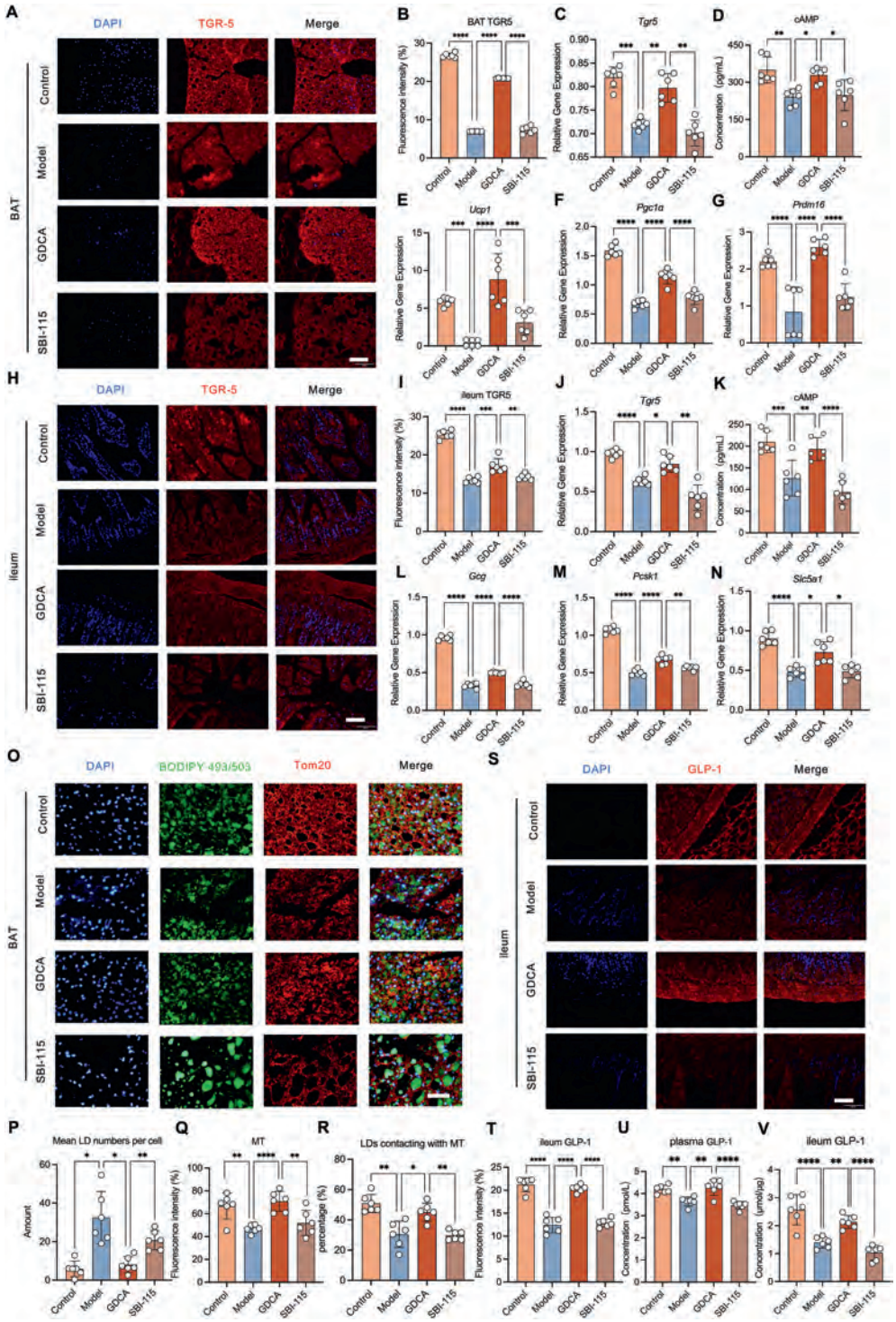

Figure 6 GDCA activated the TGR5 receptor in both brown adipose and ileum, thereby enhancing the brown adipose thermogenesis and ileal GLP-1 secretion. (A) Immunofluorescence staining and (B) quantitative analysis of fluorescence intensity of TGR5 in BAT. Gene expression of (C) *Tgr5* and (D) cAMP concentration in BAT, indicating the activation status of TGR5 signaling. Thermogenic markers of BAT, including (E) *Ucp1*, (F) *Pgc-1α*, and (G) *Prdm16*. (H) Immunofluorescence staining and (I) quantitative analysis of fluorescence intensity of TGR5 in the ileum tissue. Ileum expression of (J) *Tgr5* and (K) cAMP concentration. The expression of genes involving biosynthesis and secretion of GLP-1, including (L) *Gcg*, (M) *pcsk1*, and (N) *Slc5a1*, in the ileum tissue. (O) Immunofluorescence staining of BAT showing lipid droplets (LDs) labeled with BODIPY 493/503 and mitochondria (MT) labeled with Tom20. The significantly reduced mean LD number per cell (P), elevated MT fluorescence intensity (Q), and increased proportion of LDs-MT contact (R), collectively indicate enhanced BAT thermogenesis induced by GDCA. GDCA also boosted the levels of GLP-1, indicated by (S, T) immunofluorescence staining of the ileum, and ELISA measurements in both (U) plasma and (V) ileal samples. The data are represented as means ± SD, $n = 6$; Scale bars: 50 μm; NS for $P > 0.05$, $^{*}P < 0.05$, $^{**}P < 0.01$, $^{***}P < 0.001$, $^{****}P < 0.0001$.

luciferase assay demonstrated robust TGR5 activation by GDCA, using the selective agonist INT-777 as a positive control (Fig. 7A); this finding was supported by *Tgr5* gene expression analysis (Fig. 7B). The cAMP signaling pathway is a critical pathway regulating the UCP-1-mediated heat production in brown adipose tissue[40]. GDCA administration increased cAMP concentration dose-dependently in brown adipocytes, which could be reversed by SBI-115 (Fig. 7C), and a similar trend was observed in the TGR5 protein expression (Fig. 7G and H). GDCA improved the gene expression of *Ucp-1* and *Prdm-16*, and this effect disappeared when exposed to the TGR5-specific inhibitor SBI-115 (Fig. 7D−F). In addition, we also determined the protein expression of UCP1, PGC1α, and PRDM16 *via* Western blot and observed similar trends to those of the mRNA results (Fig. 7G−K). In short, these findings provide compelling evidence that GDCA enhances energy expenditure in brown adipocytes *via* the TGR5−cAMP pathway. This elucidates the cellular mechanism by which GDCA combats obesity and improves metabolism.

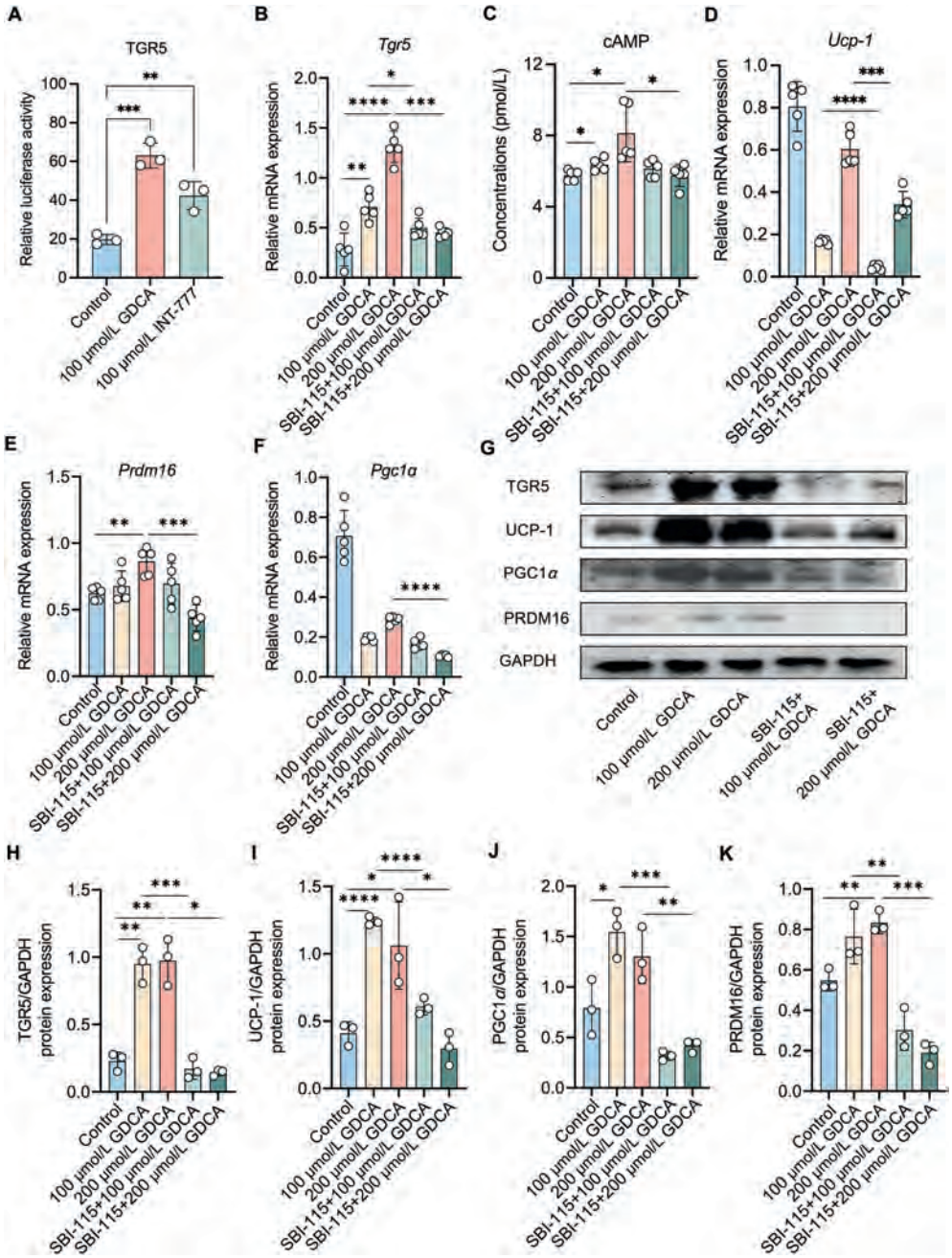

Figure 7 GDCA enhanced the thermogenic capacity of brown adipocytes in a TGR5-dependent manner. (A) Relative luciferase activity of TGR5, using the selective TGR5 agonist INT-777 as a positive control ($n = 3$). (B) Gene expression of *Tgr5*. (C) cAMP concentration. Thermogenic markers, including (D) *Ucp1*, (E) *Prdm16*, and (F) *Pgc1α* in C3H10T1/2 derived brown adipocytes treated with DMSO (control), GDCA, or GDCA + SBI-115 (TGR5 inhibitor). Western blot analyses (G) and quantification of TGR5 (H), UCP-1 (I), PGC1α (J), and PRDM16 (K) protein levels in differentiated C3H10T1/2 cells, with GAPDH used as a loading control. The data are represented as means ± SD; NS for $P >$ 0.05, $^{*}P < 0.05$, $^{**}P < 0.01$, $^{***}P < 0.001$, $^{****}P < 0.0001$.

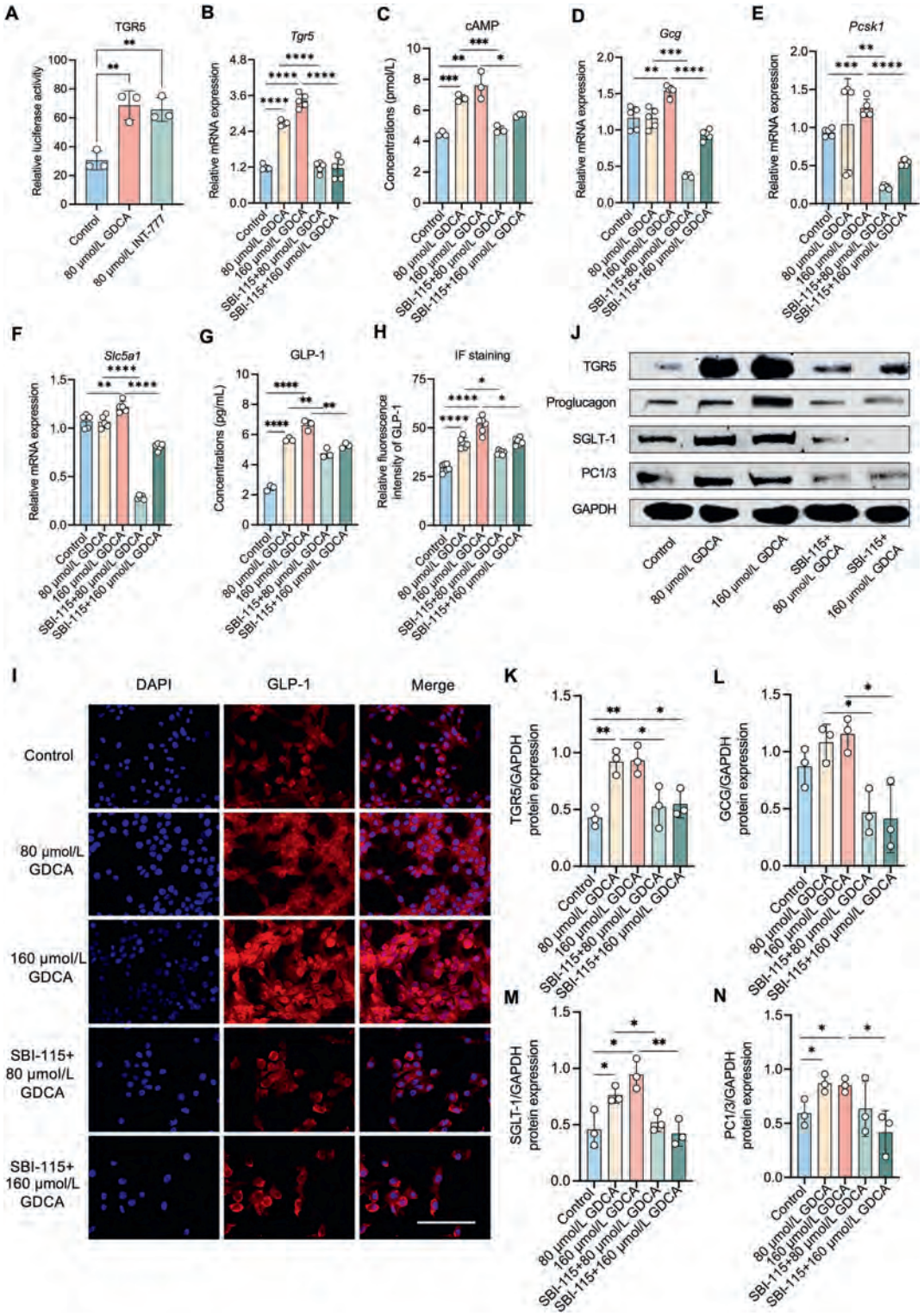

Figure 8 GDCA boosted GLP-1 secretion *via* the activation of TGR5 in STC-1 enteroendocrine cells. (A) Relative luciferase activity of TGR5, with TGR5 agonist INT-777 as a positive control ($n = 3$). (B) Gene expression of *Tgr5*. (C) cAMP concentration. Genes related to GLP-1 secretion, including (D) *Gcg*, (E) *Pcsk1*, and (F) *Slc5a1*. (G) GLP-1 concentrations measured with ELISA. (H) Quantitative analysis and (I) representative IF staining of GLP-1 expression in STC-1 cells treated with DMSO, GDCA, or GDCA + SBI-115 (scale bar: 100 μm). (J) Western blot analyses and quantitative analyses of (K) TGR5, (L) GCG, (M) SGLT1, and (N) PC1/3 protein levels in STC-1 cells. GAPDH was used as a loading control. The data are represented as means ± SD; NS for $P > 0.05$, *$P < 0.05$, **$P < 0.01$, ***$P < 0.001$, ****$P < 0.0001$.

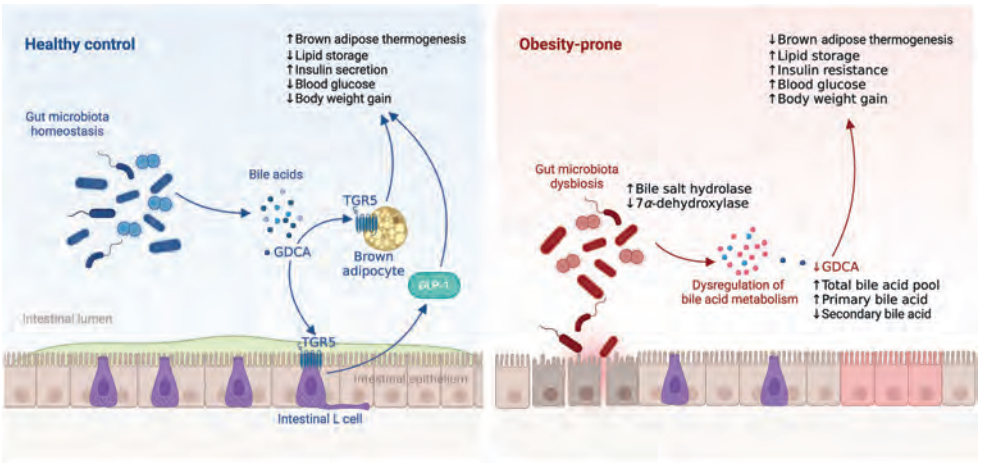

Figure 9 Schematic diagram of the present research. Metabolic disorders of the Obesity-prone individuals were due to altered gut microbiota and identified bile acid profile, especially secondary bile acid GDCA. The metabolic benefits of GDCA were involved in a TGR5-dependent fashion, including increased energy expenditure in BAT, enhanced GLP-1 secretion in the intestines, and improved lipid metabolism in adipose tissues and the liver.

We also examined how GDCA supplementation affects the secretion of GLP-1 using enteroendocrine STC-1 cells. GDCA activated the TGR5 receptor in STC-1 cells, as demonstrated by relative luciferase activity of TGR5 (Fig. 8A), up-regulated TGR5 mRNA and protein expressions (Fig. 8B−J and K), as well as increased cAMP levels (Fig. 8C). The GLP-1 production was promoted consequently by GDCA, as indicated by ELISA (Fig. 8G) and immunofluorescent staining (Fig. 8H and I). Subsequently, we further analyzed the expression of GLP-1 modulators. As expected, GDCA up-regulated the gene expression of *Gcg*, *Pcsk1*, and *Slc5a1* (Fig. 8D−F). This result was confirmed by the elevated protein levels of Proglucagon (encoded by *Gcg*), SGLT1 (encoded by *Slc5a1*), and PC1/3 (encoded by *Pcsk1*) in GDCA groups (Fig. 8J, L−N). However, all the effects were abolished by the SBI-115 intervention, which substantiated the indispensable role of TGR5 in the bioactivity of GDCA.

Collectively, the data demonstrate that GDCA effectively improves thermogenesis in brown adipocytes and boostes GLP-1 secretion in enteroendocrine STC-1 cells through the activation of TGR5−cAMP signaling, thereby exerting potent effects on the improvement of glycolipid metabolism.

4. Discussion

Obesity and its related disorders impact multiple organs and disrupt whole-body homeostasis. In addition to genetic regulation and environmental influences, an individual's inner susceptibility also plays a crucial role in obesity development. The gut microbiota and its derived BAs have been increasingly recognized as critical modulators of host metabolism. In the present study, we recruited OP individuals to investigate the underlying pathological basis of obesity susceptibility through the lens of gut microbiota and BAs. Unlike previous research focused on generalized obesity or therapeutic interventions in established disease, our work specifically targets OP individuals at a preclinical stage, prior to the onset of overt metabolic disorders. This pre-disease population is clinically significant for early identification and intervention, yet the mechanisms underlying their metabolic susceptibility remain poorly characterized.

The results demonstrated that OP individuals have metabolic disturbances intricately linked to their gut microbiota and BA profiles. The OP individuals display an elevated Firmicutes-to-Bacteroidetes ratio, and *Prevotella* was the signature genus in this population. Variations in microbial composition led to altered BA pools in OP subjects, with GDCA identified as the most potent discriminator between OP and HC groups. OP individuals exhibited a significant reduction in GDCA concentrations. Through FMT experiments, we confirmed the role of gut microbiota in modulating host glycolipid metabolism and BA profiles, particularly the decrease in GDCA. Furthermore, the supplement with GDCA exerted marked metabolic benefits in a TGR5-dependent fashion by increasing the energy expenditure in BAT and enhancing the GLP-1 secretion in the ileum[41], therefore reducing adiposity and improving glycolipid metabolic disorders (Fig. 9). These findings position GDCA as a potential biomarker for early risk stratification and a therapeutic target for preventing metabolic diseases in susceptible populations, shifting the focus from treating established obesity to preemptive intervention.

Our current study revealed a distinct gut microbiota clustering pattern between OP and HC groups, and the Firmicutes-to-Bacteroidetes ratio displayed a significant increase in OP individuals, which is in agreement with previous reports[42,43]. We identified *Prevotella* to be the signature gut microbiota genus of OP individuals, which has been previously reported to be increased in various metabolic disorders such as obesity[44,45], metabolic dysfunction-associated steatohepatitis (MASH)[46], type 2 diabetes[47], and polycystic ovary syndrome (PCOS)[48]. The FMT experiment revealed that the glycolipid metabolism disorders were attributed to the gut microbiota from OP subjects. Bacterial genera that express BSH, HSDH, and 7α-dehydroxylases play a vital role in the metabolism of secondary BAs[49]. Our study found that the OP group exhibited a significant increase in the abundance of bacterial taxa expressing BSH, while there was a decrease in those expressing 7α-dehydroxylases.

BAs serve as endogenous signaling molecules that can regulate glycolipid metabolism homeostasis and impact the regulation of energy expenditure and the development of obesity[50]. OP subjects displayed significantly remodeled both plasma and fecal BA

profiles. GDCA significantly decreased in OP individuals, and was identified as a promising biomarker candidate for identifying OP, proposing a valuable target for the early prevention and management of obesity. GDCA levels exhibited a negative correlation with body weight, BMI, waist circumference, and other metabolic indicators, and a positive association with *Tgr5*, BAT thermogenic marker genes, and GLP-1 concentrations. Previous studies have shown that GDCA is substantially reduced in PCOS subjects[29], and the diminished GDCA levels were associated with gestational diabetes mellitus[51]. Moreover, the beneficial effects of GDCA have been highlighted in a recent study, which found that the administration of GDCA decreased insulin resistance and improved glucose metabolism in PCOS-like mouse models[29]. Our investigation found that GDCA supplementation to mice fed with HFD reduced body weight and fat accumulation and improved glycolipid metabolic parameters.

TGR5 is a pivotal BA receptor that regulates glycolipid metabolism; genetic depletion of *Tgr5* impedes thermogenesis in the BAT, thus resulting in obesity in mice[52]. Consistent with this, we observed a significant reduction in the gene expression of *Tgr5* in both BAT and ileum tissues of diet-induced obesity mice. Furthermore, GDCA was found to effectively activate TGR5 signaling in both BAT and the ileum. Through both *in vivo* and *in vitro* approaches, we verified that GDCA promotes thermogenesis in the BAT and enhances the production of ileal GLP-1 in a TGR5-dependent manner. These findings indicate that microbial dysbiosis and subsequent depleted GDCA of OP individuals may contribute to their predisposition to obesity and other metabolic diseases, providing mechanistic insights into the pathogenesis of the OP phenotype.

There are several limitations in this study. First, due to medical ethics and practical constraints, we only tested blood and fecal samples but did not examine TGR5 signaling in the adipose and ileum tissues. Second, although we employed pharmacological inhibition of key targets, future studies should employ genetic knockout models to verify these findings. Finally, while antibiotic-treated mice were used to assess the role of gut microbiota in host glycolipid metabolism, results from rodent models may not be directly translatable to humans. In addition, we did not detect other gut microbiota-derived metabolites, such as short-chain fatty acids, which may also affect host glycolipid metabolism. Further studies will be required to fully understand the mechanistic links between the gut microbiota dysbiosis-induced BA composition variations and metabolic status in OP individuals.

5. Conclusions

In conclusion, our findings indicate that gut microbiota-mediated alterations in BA profiles, particularly the reduced activation of TGR5 signaling by GDCA, contribute to disturbances in host glycolipid metabolism and increased susceptibility to obesity. GDCA represents a promising biomarker for early identification and intervention in OP individuals. The strong association between BAs and metabolic status suggests that modulating BA signaling may offer a potential strategy for the early prevention and treatment of obesity.

Acknowledgments

This work was partially supported by the National Natural Science Foundation of China (Nos. 82274379 and 82474371) and the Beijing Natural Science Foundation-Daxing Innovation Foundation Joint Project (No. L246067, China).

Author contributions

Haiqiang Yao, Jin-Yi Wan, and Chun-Su Yuan contributed to the conceptualization and organization of this study. Jin-Yi Wan and Haiqiang Yao contributed to the data analysis, visualization, and writing. Han Ma, Yuqi Wu, Delong Li, Haowen Sun, Yuan Xie, Shichun Zhao, Wenqian Guo, Meng Wang, Renyun Cui, Yanrong Huang, and Xiankang Zhang contributed to the experiments, data collection, and data processing.

Conflicts of interest

The authors declare no conflicts of interest.

Appendix A. Supporting information

Supporting information to this article can be found online at https://doi.org/10.1016/j.apsb.2025.12.006.

References

1. GBD 2021 Adult BMI Collaborators. Global, regional, and national prevalence of adult overweight and obesity, 1990-2021, with forecasts to 2050: a forecasting study for the global burden of disease study 2021. *Lancet* 2025;**405**:813−38.
2. GBD 2021 Adolescent BMI Collaborators. Global, regional, and national prevalence of child and adolescent overweight and obesity, 1990−2021, with forecasts to 2050: a forecasting study for the global burden of disease study 2021. *Lancet* 2025;**405**:785−812.
3. Piché ME, Tchernof A, Després JP. Obesity phenotypes, diabetes, and cardiovascular diseases. *Circ Res* 2020;**126**:1477−500.
4. Wang CC, Lin JH, Duan M, He JL, Halizere S, Chen NX, et al. Multi-omics reveals different signatures of obesity-prone and obesity-resistant mice. *iMetaOmics* 2025;**2**:e59.
5. Kral TV. Eating behaviors and weight development in obesity-prone children and the importance of the research of Albert J. Stunkard. *Curr Obes Rep* 2016;**5**:126−31.
6. Wei ML, Huang FJ, Zhao L, Zhang YJ, Yang W, Wang SL, et al. A dysregulated bile acid−gut microbiota axis contributes to obesity susceptibility. *EBioMedicine* 2020;**55**:102766.
7. Gilbert JA, Blaser MJ, Caporaso JG, Jansson JK, Lynch SV, Knight R. Current understanding of the human microbiome. *Nat Med* 2018;**24**: 392−400.
8. Zhang ZQ, Shi XL, Ji JM, Guo YL, Peng Q, Hao LY, et al. Dihydroartemisinin increased the abundance of *Akkermansia muciniphila* by YAP1 depression that sensitizes hepatocellular carcinoma to anti-PD-1 immunotherapy. *Front Med* 2023;**17**:729−46.
9. Bäckhed F, Manchester JK, Semenkovich CF, Gordon JI. Mechanisms underlying the resistance to diet-induced obesity in germ-free mice. *Proc Natl Acad Sci U S A* 2007;**104**:979−84.
10. Rabot S, Membrez M, Bruneau A, Gérard P, Harach T, Moser M, et al. Germ-free C57BL/6J mice are resistant to high-fat-diet-induced insulin resistance and have altered cholesterol metabolism. *FASEB J* 2010;**24**:4948−59.
11. Turnbaugh PJ, Ley RE, Mahowald MA, Magrini V, Mardis ER, Gordon JI. An obesity-associated gut microbiome with increased capacity for energy harvest. *Nature* 2006;**444**:1027−31.
12. Ridaura VK, Faith JJ, Rey FE, Cheng J, Duncan AE, Kau AL, et al. Gut microbiota from twins discordant for obesity modulate metabolism in mice. *Science* 2013;**341**:1241214.

13. Wahlström A, Sayin SI, Marschall HU, Bäckhed F. Intestinal crosstalk between bile acids and microbiota and its impact on host metabolism. *Cell Metab* 2016;**24**:41−50.
14. Chávez-Talavera O, Haas J, Grzych G, Tailleux A, Staels B. Bile acid alterations in nonalcoholic fatty liver disease, obesity, insulin resistance and type 2 diabetes: what do the human studies tell?. *Curr Opin Lipidol* 2019;**30**:244−54.
15. Puri P, Daita K, Joyce A, Mirshahi F, Santhekadur PK, Cazanave S, et al. The presence and severity of nonalcoholic steatohepatitis is associated with specific changes in circulating bile acids. *Hepatology* 2018;**67**:534−48.
16. Wang SJ, Deng YY, Xie XY, Ma J, Xu M, Zhao XJ, et al. Plasma bile acid changes in type 2 diabetes correlated with insulin secretion in two-step hyperglycemic clamp. *J Diabetes* 2018;**10**:874−85.
17. Semova I, Levenson AE, Krawczyk J, Bullock K, Gearing ME, Ling AV, et al. Insulin prevents hypercholesterolemia by suppressing 12α-hydroxylated bile acids. *Circulation* 2022;**145**:969−82.
18. Haeusler RA, Astiarraga B, Camastra S, Accili D, Ferrannini E. Human insulin resistance is associated with increased plasma levels of 12α-hydroxylated bile acids. *Diabetes* 2013;**62**:4184−91.
19. van Nierop FS, Scheltema MJ, Eggink HM, Pols TW, Sonne DP, Knop FK, et al. Clinical relevance of the bile acid receptor TGR5 in metabolism. *Lancet Diabetes Endocrinol* 2017;**5**:224−33.
20. Darmanto AG, Yen TL, Jan JS, Linh TTD, Taliyan R, Yang CH, et al. Beyond metabolic messengers: bile acids and TGR5 as pharmacotherapeutic intervention for psychiatric disorders. *Pharmacol Res* 2025;**211**:107564.
21. Duboc H, Taché Y, Hofmann AF. The bile acid TGR5 membrane receptor: from basic research to clinical application. *Dig Liver Dis* 2014;**46**:302−12.
22. Lun WJ, Yan QH, Guo XH, Zhou MC, Bai Y, He JC, et al. Mechanism of action of the bile acid receptor TGR5 in obesity. *Acta Pharm Sin B* 2024;**14**:468−91.
23. Watanabe M, Houten SM, Mataki C, Christoffolete MA, Kim BW, Sato H, et al. Bile acids induce energy expenditure by promoting intracellular thyroid hormone activation. *Nature* 2006;**439**:484−9.
24. Thomas C, Gioiello A, Noriega L, Strehle A, Oury J, Rizzo G, et al. TGR5-mediated bile acid sensing controls glucose homeostasis. *Cell Metab* 2009;**10**:167−77.
25. Kuhre RE, Holst JJ, Kappe C. The regulation of function, growth and survival of GLP-1-producing L-cells. *Clin Sci* 2015;**130**:79−91.
26. Dong CY, Zhou BL, Zhao BY, Lin K, Tian YM, Zhang R, et al. GLP-1RAs attenuated obesity and reversed leptin resistance partly *via* activating the microbiome-derived inosine/A2A pathway. *Acta Pharm Sin B* 2025;**15**:1023−38.
27. Guo WQ, Zhang ZL, Li LR, Liang X, Wu YQ, Wang XL, et al. Gut microbiota induces DNA methylation *via* SCFAs predisposing obesity-prone individuals to diabetes. *Pharmacol Res* 2022;**182**:106355.
28. Li LR, Wang ZY, Wang J, Zheng YF, Li YS, Wang Q. Enlightenment about using TCM constitutions for individualized medicine and construction of Chinese-style precision medicine: research progress with TCM constitutions. *Sci China Life Sci* 2021;**64**:2092−9.
29. Qi XY, Yun CY, Sun LL, Xia JL, Wu Q, Wang Y, et al. Gut microbiota−bile acid−interleukin-22 axis orchestrates polycystic ovary syndrome. *Nat Med* 2019;**25**:1225−33.
30. Liu M, Xie WJ, Zhang X, Wu W, Li G, Wang L. Sodium butyrate regulates macrophage polarization by TGR5/β-arrestin2 *in vitro*. *Mol Med* 2025;**31**:31.
31. Wang H, Wang JX, Cui H, Fan CY, Xue YZ, Liu HY, et al. Inhibition of fatty acid uptake by TGR5 prevents diabetic cardiomyopathy. *Nat Metab* 2024;**6**:1161−77.
32. Kubota S, Yabe D. Elevation of fasting GLP-1 levels in child and adolescent obesity: friend or foe?. *J Clin Endocrinol Metab* 2021;**106**:e3778−80.
33. Seon MJ, Hwang SY, Son Y, Song J, Kim OY. Circulating GLP-1 levels as a potential indicator of metabolic syndrome risk in adult women. *Nutrients* 2021;**13**:865.
34. Pang B, Chen YB, Wang S, Yang DQ, Yu ZL, She Y, et al. World's top 50 high-impact research studies in traditional medicine in 2024. *Acupunct Herb Med* 2024;**4**:552−8.
35. Chang HW, Lee EM, Wang Y, Zhou C, Pruss KM, Henrissat S, et al. *Prevotella copri* and microbiota members mediate the beneficial effects of a therapeutic food for malnutrition. *Nat Microbiol* 2024;**9**:922−37.
36. Perino A, Schoonjans K. Metabolic messengers: bile acids. *Nat Metab* 2022;**4**:416−23.
37. Jia W, Xie GX, Jia WP. Bile acid−microbiota crosstalk in gastrointestinal inflammation and carcinogenesis. *Nat Rev Gastroenterol Hepatol* 2018;**15**:111−28.
38. Jiao N, Baker SS, Chapa-Rodriguez A, Liu WS, Nugent CA, Tsompana M, et al. Suppressed hepatic bile acid signalling despite elevated production of primary and secondary bile acids in NAFLD. *Gut* 2018;**67**:1881−91.
39. Makki K, Brolin H, Petersen N, Henricsson M, Christensen DP, Khan MT, et al. 6α-Hydroxylated bile acids mediate TGR5 signalling to improve glucose metabolism upon dietary fiber supplementation in mice. *Gut* 2022;**72**:314−24.
40. Reverte-Salisa L, Siddig S, Hildebrand S, Yao X, Zurkovic J, Jaeckstein MY, et al. EPAC1 enhances brown fat growth and beige adipogenesis. *Nat Cell Biol* 2024;**26**:113−23.
41. Yao HQ, Zhang AQ, Li DL, Wu YQ, Wang CZ, Wan JY, et al. Comparative effectiveness of GLP-1 receptor agonists on glycaemic control, body weight, and lipid profile for type 2 diabetes: systematic review and network meta-analysis. *BMJ* 2024;**384**:e076410.
42. Ley RE, Turnbaugh PJ, Klein S, Gordon JI. Microbial ecology: human gut microbes associated with obesity. *Nature* 2006;**444**:1022−3.
43. Riva A, Borgo F, Lassandro C, Verduci E, Morace G, Borghi E, et al. Pediatric obesity is associated with an altered gut microbiota and discordant shifts in Firmicutes populations. *Environ Microbiol* 2017;**19**:95−105.
44. Nirmalkar K, Murugesan S, Pizano-Zárate ML, Villalobos-Flores LE, García-González C, Morales-Hernández RM, et al. Gut microbiota and endothelial dysfunction markers in obese Mexican children and adolescents. *Nutrients* 2018;**10**:2009.
45. Thingholm LB, Rühlemann MC, Koch M, Fuqua B, Laucke G, Boehm R, et al. Obese individuals with and without type 2 diabetes show different gut microbial functional capacity and composition. *Cell Host Microbe* 2019;**26**:252-64.e10.
46. Zhu LX, Baker SS, Gill C, Liu WS, Alkhouri R, Baker RD, et al. Characterization of gut microbiomes in nonalcoholic steatohepatitis (NASH) patients: a connection between endogenous alcohol and NASH. *Hepatology* 2013;**57**:601−9.
47. Doumatey AP, Adeyemo A, Zhou J, Lei L, Adebamowo SN, Adebamowo C, et al. Gut microbiome profiles are associated with type 2 diabetes in urban Africans. *Front Cell Infect Microbiol* 2020;**10**:63.
48. Jobira B, Frank DN, Pyle L, Silveira LJ, Kelsey MM, Garcia-Reyes Y, et al. Obese adolescents with PCOS have altered biodiversity and relative abundance in gastrointestinal microbiota. *J Clin Endocrinol Metab* 2020;**105**:e2134−44.
49. Fuchs CD, Trauner M. Role of bile acids and their receptors in gastrointestinal and hepatic pathophysiology. *Nat Rev Gastroenterol Hepatol* 2022;**19**:432−50.
50. Molinaro A, Wahlström A, Marschall HU. Role of bile acids in metabolic control. *Trends Endocrinol Metab* 2018;**29**:31−41.
51. Zhu B, Ma ZX, Zhu YN, Fang L, Zhang H, Kong HW, et al. Reduced glycodeoxycholic acid levels are associated with negative clinical outcomes of gestational diabetes mellitus. *J Zhejiang Univ - Sci B* 2021;**22**:223−32.
52. Velazquez-Villegas LA, Perino A, Lemos V, Zietak M, Nomura M, Pols TWH, et al. TGR5 signalling promotes mitochondrial fission and beige remodelling of white adipose tissue. *Nat Commun* 2018;**9**:245.